Nuclear Materials and Energy 36 (2023) 101504

Contents lists available at ScienceDirect

Nuclear Materials and Energy

journal homepage: www.elsevier.com/locate/nme

# Hydrogen trapping in vanadium carbide alloyed with transition metals

Shuai Tang [a,*], Linxian Li [a], Haile Yan [b], Jianfeng Jin [b], Qing Peng [c,d,*], Minghui Cai [a,e], Jianping Li [a], Zhenyu Liu [b], Guodong Wang [a]

[a] State Key Lab of Rolling and Automation, Northeastern University, Shenyang 110819, China
[b] School of Materials Science and Engineering, Northeastern University, Shenyang 110819, China
[c] State Key Laboratory of Nonlinear Mechanics, Institute of Mechanics, Chinese Academy of Sciences, Beijing 100190, China
[d] School of Engineering Sciences, University of Chinese Academy of Sciences, Beijing 100049, China
[e] Key Lab of Lightweight Structural Materials, Liaoning Province, Northeastern University, Shenyang 110819, China

ARTICLE INFO

*Keywords:*
Hydrogen barrier coating
Vanadium carbide
First-principles calculations
Transition-metal alloying

ABSTRACT

The mechanism of hydrogen trapping in carbides via transition metal alloying is essential for material design of hydrogen barrier coatings in hydrogen energy applications, which however, is still elusive. Herein we have investigated the effect of transition metal solutes (Ti, Cr, Zr, Nb, and Mo) doping on multiple hydrogen trapping in vanadium carbide using density functional theory calculations. The hydrogen binding energetics with alloying elements depends on the local atomic environment of neighboring interstitial sites. The hydrogen trapping ability is ordered by Cr > Zr > Nb > Ti > Mo. Cr dopant has a distinctive performance, because its first-nearest-neighbor trigonal interstitial sites are more stable, and up to six hydrogen atoms can be trapped, surpassing other elements. This distinction is partially attributed to less lattice contractive distortion and lower loss of charge. Charge transfer and electronic analysis indicate that C—H interactions play a critical role in hydrogen binding energies. The stability of multiple hydrogen could be measured by the length and strength of the C—H bond.

## Introduction

Hydrogen can significantly affect the properties of structural materials [1–5]. With severe neutron irradiation in fusion reactors, structural materials contain large amounts of hydrogen [6,7], and the penetration of hydrogen atoms is inevitable. In addition to the leakage the precious tritium, hydrogen embrittlement is a critical concern. Applying hydrogen barrier coatings with a high permeation reduction factor (HPRF) can effectively resist the intrusion of hydrogen atoms and the tritium uptake without damaging the substrate [8,9]. It has been shown that vanadium carbide (VC) coatings have a lower hydrogen diffusion coefficient [10] and reduced chemical interaction with the fuel cladding compared to conventional $Al_2O_3$ [11]. Moreover, VC coatings also significantly improve the hardness and wear resistance of the substrate [12–14]. Therefore, VC is an attractive hydrogen barrier material [15]. Enhanced performance under high-energy neutron irradiation is an essential concern of VC hydrogen barrier coatings.

Generally, the permeation reduction factor is modified by the trapped hydrogen atoms at lattice defects (e.g., vacancies, solute atoms) [16–18]. Although the strong attraction of vacancies increases the solubility of hydrogen [19], hydrogen diffusion becomes easier with increasing vacancy content [15]. Studies have shown that doping elements enhance hydrogen trapping and retard hydrogen diffusion [20,21]. Kim et al. [22] found that hydrogen permeability was reduced by 80 % in carbon-doped TiZrN coating. The findings from Somjit et al. [23] showed that doping with Si and Ti at 1 ppm can significantly reduce the hydrogen solubility and diffusion rate in $Al_2O_3$. A large number of trapping sites in the VC crystal structure weaken hydrogen diffusion and significantly diminish hydrogen embrittlement sensitivity [24,25]. Nagao et al. [26] found that hydrogen embrittlement was lessened due to Mo-doped TiC in martensitic steels. Dey et al. [27] found a linear relationship between hydrogen solubility and doped Cr content in $Fe_3C$ and $Fe_{23}C_6$. Elemental doping is a critical factor in improving the hydrogen trapping of carbides [28,29]. It also improves performance in terms of strength, wears resistance, and creep resistance [30–33]. For doping VC, previous investigations have been focused mainly on mechanical properties. Sun et al. [34] pointed out that (V, M)C (M = W, Mo, Cr) has better performance in terms of thermal and mechanical stability

* Corresponding authors at: State Key Lab of Rolling and Automation, Northeastern University, Shenyang 110819, China (S. Tang). State Key Laboratory of Nonlinear Mechanics, Institute of Mechanics, Chinese Academy of Sciences, Beijing 100190, China (Q. Peng).
*E-mail addresses:* tangshuai@ral.neu.edu.cn (S. Tang), pengqing@imech.ac.cn (Q. Peng).

https://doi.org/10.1016/j.nme.2023.101504
Received 26 July 2023; Received in revised form 31 August 2023; Accepted 7 September 2023
Available online 9 September 2023

and better ductility along with high hardness than pristine VC. Sangiovanni et al. [35] highlighted that (V, Nb, Ta, Mo, W)C high-entropy carbides are highly ductile at room and high temperatures. All these efforts suggest that the enhanced trapping of hydrogen by doped atoms promotes the performance of hydrogen barrier coatings. However, the interaction of doping with hydrogen in VC is still in the mist.

Because hydrogen trapping behavior is relatively difficult to measure in experiment [36,37], theoretical investigation is more feasible [38]. In recent years, density functional theory (DFT) has been successfully applied to quantitatively estimate the interaction of doped atoms with hydrogen in metals [39,40]. Qin et al. [41] showed that the solubility of hydrogen was reduced, and the diffusion activation energy was increased by the doping of Ni in the body-centered cubic (BCC) phase of vanadium. Jiang et al. [42] found that the hydrogen trapping ability of neighbor sites near the solute atom was enhanced in Ti-doped W alloys. The hydrogen trapping mechanisms in the lattice defects of pure metals have been sufficiently explored [43–46]. Charge density was effective for a number of trapping sites in pristine metals [47]. Trapped H in metals can gain electrons. In addition, the lack of charge supply can make the hydrogen cluster unstable. For the origin of hydrogen trapping at phase boundaries between BCC-Fe and NaCl-type carbides, Zhang et al. [48] proposed that the Bader volume of hydrogen can quantify hydrogen trapping, where both chemical and mechanical contributions are considered. However, VC has more complex local atomic environments containing mixed metallic, ionic, and covalent bonds [49]. The origin of multiple hydrogen trapping when doped atoms are involved is less studied. Whether the Bader atomic volume of hydrogen and charge density developed for pristine metals and phase boundaries are still sufficient to assess multiple hydrogen-binding energetics for doping elements desires further exploration.

In this paper, the hydrogen trapping behaviors of five transition metal elements –Ti, Cr, Zr, Nb, Mo – alloyed in VC have been investigated using first-principles calculations. These elements are selected because they can form NaCl-type carbides and they are common additives in steels. Our investigation has three steps. Firstly, the maximum interaction distance between solute atoms and a hydrogen atom (M—H pair) and the optimal trapping sites is calculated using the hydrogen binding energy. Secondly, the hydrogen bonding ability between neighboring hydrogen atoms (H-H pair) and the farthest interaction distance is discussed. Finally, the maximum number of multiple hydrogen atoms trapped near the solute atoms (M−*n*H complexion) and the electronic characterization are investigated.

## Methods

First-principles calculations were carried out using Vienna ab initio simulation package (VASP) [50]. The core electrons were considered by the projector augmented wave (PAW) method [51]. The exchange–correlation potential was simulated using Perdew-Burke-Ernzerhof (PBE) [52] in the framework of the generalized gradient approximation (GGA) [53]. The valence electrons of Ti, V, Cr, Zr, Nb, Mo, C and H are $3s^23p^63d^24s^2$, $3s^23p^63d^44s^1$, $3p^63d^54s^1$, $4s^24p^64d^25s^2$, $4s^24p^64d^45s^1$, $4s^24p^64d^55s^1$, $2s^22p^2$ and $1s^1$ electrons, respectively. The VC model is a 2 × 2 × 2 supercell with 64 atoms, where cell size and atomic positions are allowed to relax until the energy change on each atom converged to $10^{-5}$ eV/atom the residual force was less than 0.01 eV/Å. The 4 × 4 × 4 *k*-mesh was applied to VC supercell which is based on the Monkhorst-Pack [54] method, and its accuracy is verified in Fig. S1 of Supplementary Materials. The cutoff energy of the plane waves is 520 eV. The zero-point energy correction is not considered [55] because it has little effect on the stability comparison, as shown in Table S1 of Supplementary Materials. The crystal and electronic structures was visualized by VESTA [56]. The charge analysis was obtained by Bader code [57]. The crystal orbital Hamiltonian population (COHP) was calculated by LOBSTER [58] to analyze the strength of chemical bonds.

The hydrogen atom solution energy ($E_{sol}$) when hydrogen atom occupies different interstitial can measure the solubility of hydrogen atom. $E_{sol}$ is defined as [59]:

$$E_{sol} = E_{VC,H} - E_{VC} - 1/2E_{H_2}, \tag{1}$$

where $E_{VC,H}$ is the energy of VC when the trapped hydrogen atom occupies interstitial sites, $E_{VC}$ is the energy of VC, while $E_{H_2}$ is the energy of the independent hydrogen molecule in free space.

When the VC supercell contains an M atom (M = Ti, Cr, Zr, Nb, Mo) and *n* hydrogen atoms ($n \geq 1$, and *n* is an integer), the binding energy $E_b^{M,nH}$ can describe the strength of the M atom binding to the *n*th hydrogen atom, as expressed:

$$E_b^{M,nH} = \left(E_{VC,H} - E_{VC}\right) - \left(E_{M,nH} - E_{M,(n-1)H}\right), \tag{2}$$

where $E_{VC,H}$ is the energy of VC when the hydrogen atom occupies the most stable trapping site, and $E_{M,nH}$ is the energy of the VC containing a M atom and *n* hydrogen atoms. The positive binding energy indicates that the system can enhance the trapping of *n* hydrogen atoms, while the negative value indicates that the system can enhance the trapping of up to (*n*-1) hydrogen atoms.

The binding energy $E_b^{H,H}$ can describe the strength of the binding of two hydrogen atoms. $E_b^{H,H}$ is defined as [60,61]:

$$E_b^{H,H} = \left(E_{VC,H} - E_{VC}\right) - \left(E_{VC,2H} - E_{VC,H}\right), \tag{3}$$

where $E_{VC,2H}$ is the energy of the VC containing two hydrogen atoms.

To analyze the binding ability between solute atom (Ti, Cr, Zr, Nb, Mo) and the *n*th hydrogen atom as well as between two hydrogen atoms in detail, $E_b^{M,nH}$ and $E_b^{H,H}$ are divided into the mechanical ($E_b^{mech}$) and chemical ($E_b^{chem}$) effects [62–67]. The mechanical effect is the energy effect of local strain resulting from the *n*th hydrogen atom to binding energy, and the chemical effect is the energy effect of the local chemical environment in which the *n*th hydrogen atom to the binding energy.

$$E_{b,M-nH}^{mech} = \left(E_{VC,H}^{u} - E_{VC}\right) - \left(E_{M,nH}^{u} - E_{M,(n-1)H}^{u}\right), \tag{4}$$

$$E_{b,H-H}^{mech} = \left(E_{VC,H}^{u} - E_{VC}\right) - \left(E_{VC,2H}^{u} - E_{VC,H}^{u}\right), \tag{5}$$

$$E_{b,M-nH}^{chem} = E_b^{M,nH} - E_{b,M-nH}^{mech}, \tag{6}$$

$$E_{b,H-H}^{chem} = E_b^{H,H} - E_{b,H-H}^{mech}, \tag{7}$$

where $E_{VC,H}^{u}(E_{VC,2H}^{u})$ is the energy of the hypothetical VC supercell after removing the most stable hydrogen atom (two hydrogen atoms) in VC, while $E_{M,nH}^{u}$ is the energy of the hypothetical VC supercell containing M atom after removing *n* hydrogen atoms in VC, which are obtained by self-consistent calculations for the system after removing *n* hydrogen atoms. Since hydrogen atoms are removed, hydrogen atoms no longer chemically interact with other atoms. Consequently, this equation (4) and (5) does not account for the chemical effect of hydrogen binding energy.

## Results and discussion

### *Interaction between the solute and H*

#### *Binding energy of M—H pair*

The space group of the VC crystal structure is Fm $\bar{3}$ m (No. 225), and VC is a NaCl-type face-centered cubic structure. The lattice constant after VC lattice optimization (4.16 Å) is consistent with the experimental [68] and calculated [15,69] values. The formation energies of these five transition metal elements (Ti, Cr, Zr, Nb, Mo) in VC are all negative, indicating that they can be easily doped into VC, as shown in Table S2 of Supplementary Materials. The possible sites occupied by hydrogen atom are considered as follows: the hydrogen atom occupies the center of four

neighboring V atoms (tetrahedral interstitial site, termed as Tet-V), and the hydrogen atom occupies the center of three neighboring V atoms (trigonal interstitial site, termed as Tri-V). Their corresponding configurations are mapped in Fig. 1(a) and (b). The solution energy of hydrogen atom present in the Tri-V site is 1.53 eV, which is lower than that of the Tet-V site (2.06 eV). Therefore, hydrogen atoms located at the Tri-V site are more stable, consistent with the literature [24,25].

When the V atom is replaced by the solute atom M, the first nearest neighbor tetrahedral (Tet-$V_M^{1NN}$) or trigonal (Tri-$V_M^{1NN}$) interstitial site is examined. Their corresponding configurations are mapped in Fig. 1(c) and (d). However, the hydrogen atoms occupying Tet-$V_M^{1NN}$ site, except for solute Cr, relaxed to Tri-$V_M^{2NN}$ site after optimization. When the solute atom is Cr, the hydrogen binding energy of Tet-$V_M^{1NN}$ site (−0.37 eV) is smaller than that of Tri-$V_M^{1NN}$ site (0.14 eV). Therefore, only the trigonal interstitial sites near the solute atom occupied by the hydrogen atom were considered in the subsequent calculations.

For the interaction of a single hydrogen atom occupying the trigonal interstitial with the solute atom, the configuration as in Fig. 2(a) is established (Tri-$V_M^{nNN}$), considering the effect of the distance of the solute atom from the first to the fifth nearest neighbor (1NN to 5NN) on the binding energy, respectively. The results are mapped in Fig. 2(b). The binding energy of M—H pair, except for Cr, reaches its maximum at the Tri-$V_M^{2NN}$ site. The binding energy is the largest when hydrogen occupies the Tri-$V_{Cr}^{1NN}$ site near Cr. Only Ti and Zr show positive binding energies with hydrogen atoms at different distances among the five solutes. The binding energy is positive when hydrogen atom is located in the Tri-$V_{Zr}^{5NN}$ site of Zr. The binding energy of the Tri-$V_M^{5NN}$ sites of the other solutes (Ti, Nb, Mo, Cr) is close to zero. The interaction between hydrogen and solute nearly disappears. If the trapping sites with the largest binding energy near the solute atoms are considered separately, there is an attraction between solute atoms and hydrogen. Therefore, the solute atoms can improve the hydrogen trapping ability of VC. The order of the enhanced ability of the solute atoms is: Cr > Zr > Nb > Ti > Mo.

In order to uncover the mechanism of the influence of solute atoms on the hydrogen trapping behavior of VC, the binding energy is divided into two parts to reflect the chemical and mechanical effects. The results of the chemical and mechanical effects are displayed in Fig. 2(c) and (d). The changing trend of binding energy is consistent with the chemical effect, implying that the chemical effect dominates binding energy. The influence of the solute atoms on the binding energy is mainly due to the change in the chemical environment by the solute atoms. The mechanical effect has an opposite trend to binding energy, inhibiting the change in binding energy. The mechanical effects due to each solute are very close at the Tri-$V_M^{4NN}$ and Tri-$V_M^{5NN}$ sites, indicating that the influence of lattice distortion caused by the interaction between solute and hydrogen atoms has disappeared.

*Electronic structures of M—H pair*

In order to discover the reason why the stable hydrogen trapping sites around the solute atoms are different, the charge transfer ($\Delta Q_M^{loss} = Q_V^{loss} - Q_M^{loss}$) and the atomic radius difference ($\Delta R_M = R_M - R_V$) between the solute atom and V atom in VC were calculated, as shown in Fig. 3. The solute atoms (Ti, Zr, Nb, and Mo) with similar trends in the above discussion lose more charge than V atoms without doping. The order of the charge loss of these solute atoms is consistent with the order of the enhanced trapping ability of solute atoms. Only Cr atom loses less charge than V atom. This allows more charge to be transferred from Cr to hydrogen atoms. Furthermore, the atomic radius of Cr is smaller than V, while the atomic radius of other solutes (Ti, Zr, Nb, and Mo) are larger than V. This leads to lattice compression caused by doping of Cr atoms, as opposed to the lattice expansion caused by other solute atoms. As a consequence, the lattice distortion caused by Cr atoms is different from that of other solute atoms. Zhang et al. [70] also concluded that the elastic energy and atomic radius difference would have an important influence on the forming phases in high entropy alloys. Therefore, the difference in the most stable trapping site of hydrogen atom near the solute atom (Tri-$V_M^{1NN}$ or Tri-$V_M^{2NN}$) is due to the difference in charge transfer and lattice distortion caused by solute atoms, which changes the environment where hydrogen atom is located.

Since the hydrogen binding energy is dominated by the chemical effect, the electron interactions between hydrogen atoms and surrounding atoms are linked to the trapping of hydrogen atoms. To further analyze the bonding of hydrogen atom to the surrounding atoms, the partial density of state (PDOS) of the hydrogen atom and the 1NN atom (C, V, M) is mapped in Fig. 4. The Tri-$V_M^{1NN}$ and Tri-$V_M^{2NN}$ sites of the doped atoms (Nb, Cr) are scrutinized. The strong hybridization of $H_s$ with $C_{2s}$ and $C_{2p}$ orbitals occurs in the energy level range of −15 eV to −10 eV and −8 eV to −5 eV, respectively. In contrast, the metal and hydrogen atoms have only weak hybridization in these two energy level ranges. Thus, there is a relationship between the strong C—H bond and the stability of hydrogen atom.

*H-H pair in pristine VC*

Before further study of the binding ability of the solute atoms to multiple hydrogen atoms, the interaction of two hydrogen atoms in the pristine VC was explored. The change in binding energy for two hydrogen atoms at different separation is considered. hydrogen atoms can occupy both trigonal and tetrahedral interstitial sites. Therefore, there are three possible situations for two hydrogen atoms: (1) both hydrogen atoms occupy the trigonal interstitial (Tri-Tri); (2) two hydrogen atoms occupy the trigonal and the tetrahedral interstitial, respectively (Tri-Tet); and (3) both hydrogen atoms occupy the tetrahedral interstitial (Tet-Tet). The distance ($d$) and the distance change ($\Delta d$) of the H-H pair after optimization are shown in Fig. 5(a). The initial H-H pair are unstable when $\Delta d$ is larger than 0.4 Å, hydrogen atoms energetically favorite other sites. Hydrogen atoms are stable in the Tri-Tri configuration. For the Tri-Tet and Tet-Tet configurations, it is stable only when the distance between two hydrogen atoms is 3.00 Å in the Tri-Tet configuration and 3.60 Å in the Tet-Tet configuration. For all configurations, the optimized H-H pair distance is greater than the bond

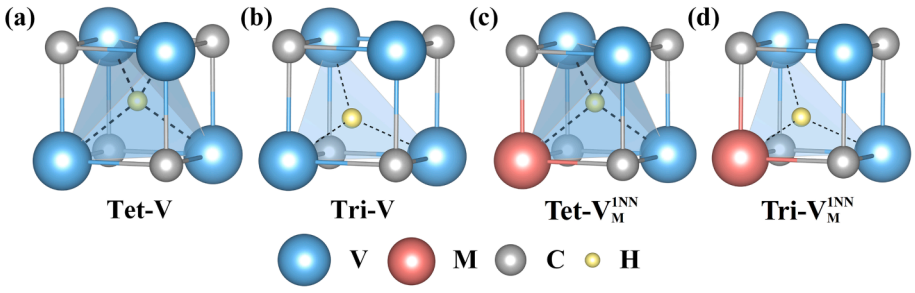


**Fig. 1.** The four types of interstitial H configurations in VC. Tetrahedral (a) and trigonal (b) interstitial sites in pristine VC. Tetrahedral (c) and trigonal (d) interstitial sites near solute atom.

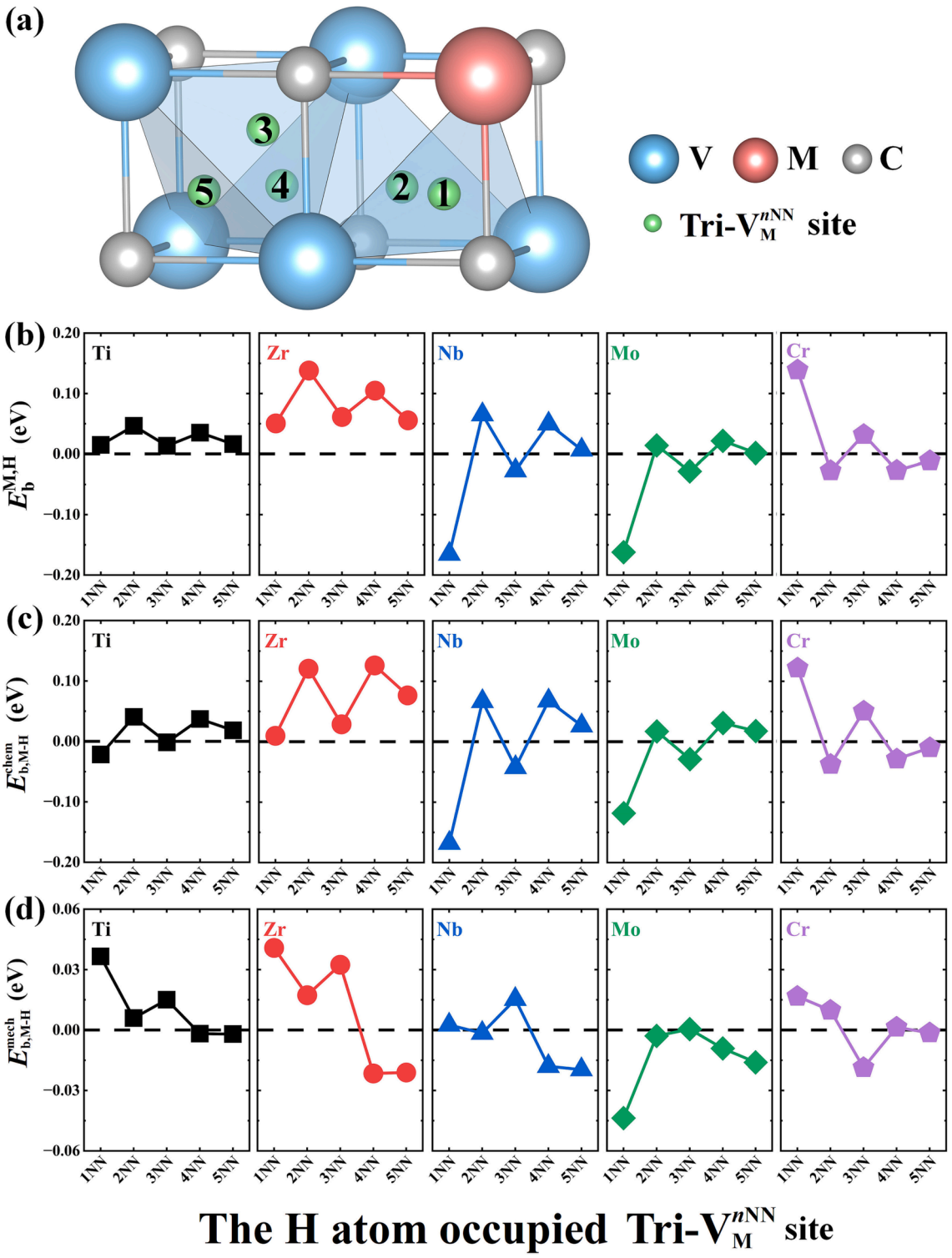


**Fig. 2.** The configuration and corresponding energies of M—H pair. (a) M—H pair at different distances. (b) binding energy, (c) chemical and (d) mechanical effects of M—H pair at different trapping sites.

length of hydrogen molecules of 0.74 Å. It might suggest that hydrogen molecules are energetically unfavorable to be formed in VC. Most hydrogen atoms occupying the tetrahedral interstitial in the H-H pair are unstable and deviate from the tetrahedral interstitial or move to the trigonal interstitial after relaxation.

The binding energies between two hydrogen atoms in the optimized stable configuration and their corresponding chemical effect and mechanical effect are illustrated in Fig. 5(b)-(c). The binding energy between two hydrogen atoms is also dominated by the chemical effect. When the binding energy is too large or too small (1.38 Å, 1.77 Å, 2.28 Å, 2.88 Å, and 3.10 Å), the distance difference between the H-H pair before and after optimization is large (greater than 0.11 Å). This is due to the strong repulsion or attraction between two hydrogen atoms. The interaction depends on the seperation of the two hydrogen atoms, which could be classified into four regions. When the distance between hydrogen atoms is in region I, the main reason why the binding energy is

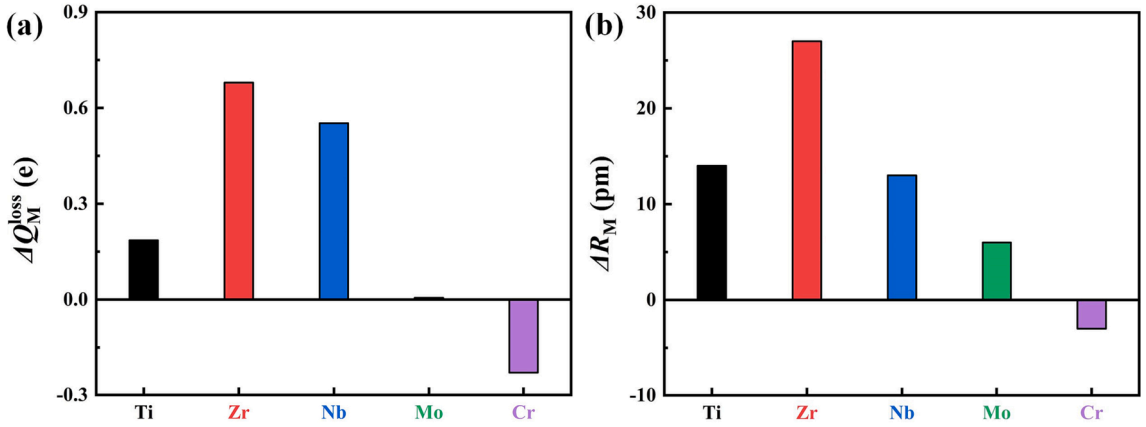


**Fig. 3.** Charge transfer and atomic radius for doping elements in VC before the addition of hydrogen atom. (a) Charge transfer ($\Delta Q_M^{loss}$) and (b) atomic radius ($\Delta R_M$) difference between the solute atom and V atom of perfect VC.

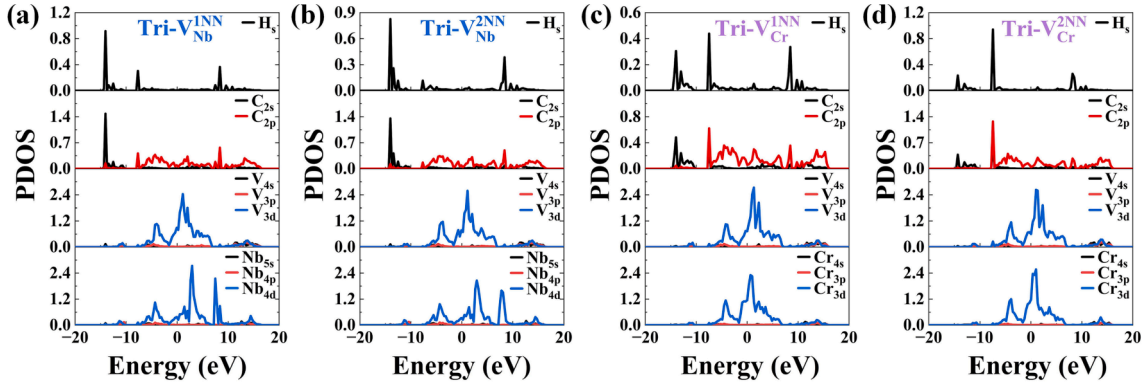


**Fig. 4.** The PDOS after hydrogen atom is located in the Tri-$V_M^{1NN}$ and Tri-$V_M^{2NN}$ sites of doped atoms (Nb, Cr). (a) Tri-$V_{Nb}^{1NN}$, (b) Tri-$V_{Nb}^{2NN}$, (c) Tri-$V_{Cr}^{1NN}$, (d) Tri-$V_{Cr}^{2NN}$.

less than zero is that the repulsion between hydrogen atoms leads to excessive lattice distortion. As a result, the negative mechanical effect weakens the binding energy. The decrease in mechanical effect at $d_{C-2H}^{1NN}$, $d_{C-2H}^{2NN}$ and $d_{C-2H}^{3NN}$ is caused by two hydrogen atoms occupying sites near the same carbon atom, whose configurations are shown in Fig. 5(d). When the H-H pair distance is in region II, the electron attraction produced by the chemical effect is greater than the elastic repulsion caused by the mechanical effect, resulting in attraction. When the H-H pair distance is in region III, the electron repulsion from chemical effects is greater than the elastic force caused by mechanical effects, thus exhibit repulsion. When the H-H pair distance is in region IV, their interactions converge to zero. In brief, the combination of mechanical and chemical effects makes the interaction between the two hydrogen atoms show an overall trend of repulsion, attraction, repulsion, and finally disappearance. The difference from the change rule of H-H pair interactions in other metals [71,72] (first repulsion, then convergence to zero) may be due to the addition of the carbon atom in the VC changing the chemical environment in which the hydrogen atoms are located.

### *Interaction between the M and multiple hydrogen atoms*

#### *Binding energy of the M−nH complexion*

Due to the strong attraction of solute atoms to hydrogen atoms, the ability of solute atoms to enhance the multiple hydrogen atoms trapping is also a vital issue. Therefore, the behavior of hydrogen atoms trapping around solute atoms is inspected. It is difficult for hydrogen atoms to exist stably in the Tet-V site due to multiple hydrogen atoms. Therefore, in addition to Cr, multiple hydrogen atoms are placed in the 2NN trigonal interstitial around the solute atom (Ti, Zr, Nb, and Mo), while hydrogen atoms occupy the 1NN trigonal interstitial around Cr, forming the M−*n*H complexion. The most stable configurations of the M−*n*H complexion are shown in Fig. 6(d)-(e), which is obtained by structural optimization of all possible M−*n*H configurations based on the M−(*n*-1) H configurations and screening for the most stable M−*n*H configurations with the largest binding energy.

The *n*th hydrogen binding energy is exhibited in Fig. 6(a)-(c). The results show that the stable configurations of the M−*n*H complexion for the solute atoms (Mo, Nb, Ti, and Zr) are consistent, with a similar trend in binding energy. The solute atoms (Mo, Nb, Ti, and Zr) can stably trap four hydrogen atoms, while Cr can stably trap six hydrogen atoms. The most stable configuration of the solute (Ti, Zr, Nb, and Mo)–*n*H complexion is shown in Fig. 6(d), and the solute (Cr)–*n*H complexion is mapped in Fig. 6(e). Considering the *n*th hydrogen binding energy and the amount of hydrogen atoms trapped, the order in which solute atoms improve the hydrogen trapping capacity of VC is Cr > Zr > Nb > Ti > Mo.

The mechanical and chemical effects of the solute atom with the *n*th hydrogen atom are shown in Fig. 6(b)-(c). The chemical effect still dominates the binding energy. The changing trend of the mechanical effect is opposite to the binding energy, weakening the influence of binding energy. The abrupt changes in the binding energy and mechanical effects of the solute atom Cr with the 2nd and 4th hydrogen atoms are due to the excessive distortion of the 2nd and 4th hydrogen atoms by sharing a carbon atom with another hydrogen atom. In brief, the solute atoms (Ti, Zr, Nb, Mo, and Cr) can improve the hydrogen trapping capacity of VC by modulating the hydrogen trapping sites. The doping of alloying elements can reduce the hydrogen permeability of the VC matrix by increasing the number of hydrogen trapped in the lattice,

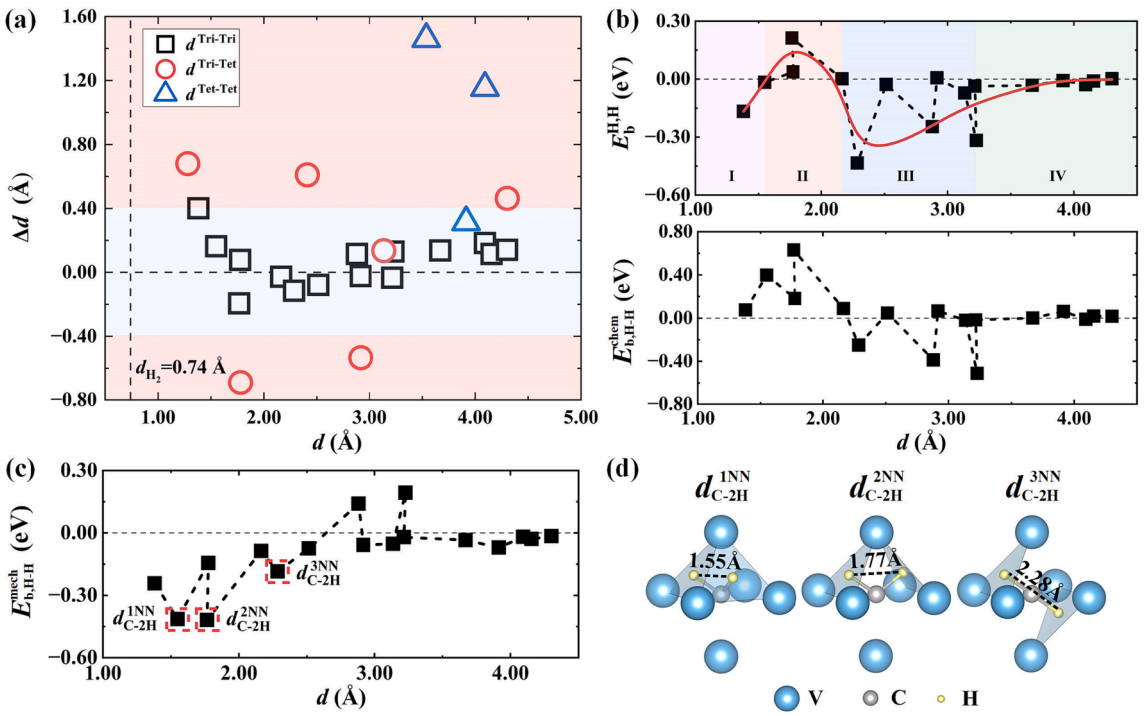


**Fig. 5.** H-H pair behavior at different distances in VC. (a) Distance change (Δ*d*) and distance (*d*) of the optimized H-H pair. (b) Binding energy, chemical effects, and (c) mechanical effects of the stable H-H pair in VC at different optimized distances. (d) The corresponding H-H pair configurations of $d_{C-2H}^{1NN}$, $d_{C-2H}^{2NN}$ and $d_{C-2H}^{3NN}$ after optimization in Fig. 5(c). $d_{H_2}$ represents the bond length of the hydrogen molecule in (a). Regions I-IV in (b) represents the interactions between hydrogen atoms which are repulsive, attractive, repulsive, and converging to zero, respectively.

of which Cr is a good alloying element. Experiments have also found that the multi-component carbides formed by V, Cr, and Mo can improve the hydrogen embrittlement resistance of the material [73–75]. Therefore, our results agree qualitatively with experiment.

*Electronic structures of the M−nH complexion*

Another important question is why the *n*th hydrogen atom is unstable. The charge transfer of (*n*-1) stable hydrogen atoms and the *n*-th unstable hydrogen atom under the most stable configuration of the M−*n*H complexion are presented in Fig. 7(a). The hydrogen atoms receive charge ($Q_{nH}^{receive}$) on the whole, as the charge received by the 5th unstable hydrogen atom of solute atoms (Ti, Zr, Nb, and Mo) is less than that received by the first four stable hydrogen atoms. In contrast, the 2nd and 3rd hydrogen atoms of Cr receive little charge due to sharing the carbon atom with other hydrogen atoms. However, the 1st and 4th hydrogen atoms get a lot of charges, which may account for the large increase in chemical effects with the addition of the second 2nd and 4th hydrogen atoms in Fig. 6(b). This allows them to occupy the site stably even if they share a carbon atom with another hydrogen atom. Therefore, the stability of hydrogen atoms is affected by the chemical environment in which they are located.

The Bader volume of hydrogen ($V_{nH}^{Bader}$) is further analyzed, because it reflects the charge characteristics in different chemical environments through the zero-flux surface of charge density [48], as shown in Fig. 7 (b). Except for the 2nd and 3rd hydrogen atoms in Cr that share a carbon atom with other hydrogen atoms, the Bader volume of the *n*th unstable hydrogen atom is smaller than the stable hydrogen atom. When the solute atom is Cr, the average Bader volume of two stable hydrogen atoms sharing a carbon atom (1st and 2nd hydrogen atoms, 3rd and 4th hydrogen atoms) are also larger than that of the 7th unstable hydrogen atom. These results reveal that for the solute atoms Ti, Zr, Nb, and Mo, the charge transfer of hydrogen atom and its corresponding Bader atomic volume can explain the reason why the *n*th hydrogen atom is unstable. However, due to the presence of two stable hydrogen atoms sharing a carbon atom in the stable configuration of Cr-*n*H complexion, these two descriptors are still not effective. Thus further discussion is needed as follows.

The results of PDOS analysis in Fig. 4 indicate that the hydrogen atoms mainly strongly hybridize to the 1NN carbon atoms. To quantitatively analyze the bonding properties of hydrogen atoms to the 1NN atom (C, V, M), the COHP analysis of the M−*n*H complexion is illustrated in Fig. 8. Both stable and unstable hydrogen atoms in the M−*n*H complexion mainly form bonds with the 1NN carbon atoms, and the strength of C—H bonds is much stronger than that of M—H bond and V—H bond. Therefore, analysis of PDOS and COHP can confirm that the C—H bond between the hydrogen atom and the 1NN carbon atom is the key factor determining whether the trapped hydrogen atom is stable.

Since the charge transfer of the hydrogen atom is affected by the neighboring carbon atom and the hydrogen atom mainly bonds with the 1NN carbon atom, the electron transfer of the 1NN carbon atom of hydrogen atom ($Q_C^{loss}$, which is defined as the charge transfer of the carbon atom before and after hydrogenation) is discussed, as shown in Fig. 9(a). The 1NN carbon atoms of the unstable hydrogen atom of the solute atom loose less charge than the 1NN carbon atoms of the stable hydrogen atom. This results in the charge received by the stable hydrogen atom and its corresponding Bader atomic volume being larger than that of the unstable hydrogen atom. The charge transfer of the solute atom affects hydrogen trapping, as illustrated in Fig. 5(b). Through the above analysis, it can be judged that the solute atom controls the charge available to hydrogen atom by influencing the charge of carbon atom around the transition metal atom, which in turn has an indirect effect on hydrogen trapping. Therefore, the stability of hydrogen atom is closely related to the charge transfer from carbon atom to hydrogen atom.

The variation of the C—H bond length ($L_{C-H}$) is further examined, as shown in Fig. 9(b). The C—H bond length of the unstable hydrogen atom is longer than that of stable hydrogen atoms. This means that the unstable hydrogen atom deviates from the stable hydrogen trapping site.

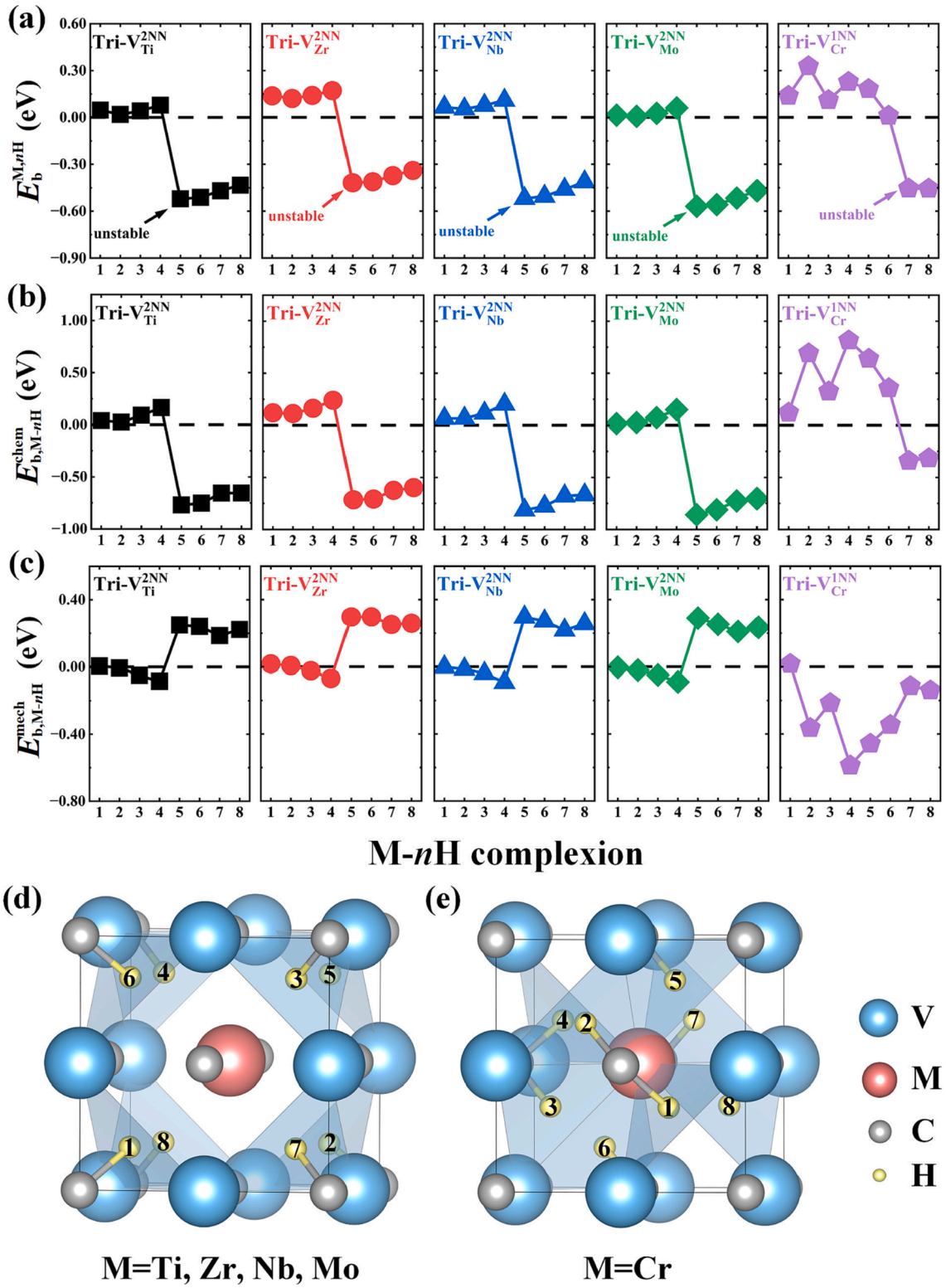


**Fig. 6.** The trapping behavior of hydrogen atoms in M–*n*H complexion. (a) Binding energy, (b) chemical and (c) mechanical effects of the solute atom with the *n*th hydrogen atom. The most stable configuration of the solute (Ti, Zr, Nb, and Mo)–*n*H complexion (d) and Cr-*n*H complexion (e). Here, the numbers indicate the *n*th hydrogen atom added.

Therefore, solute atoms can no longer trap the hydrogen atom stably. Finally, the change of bond length also alters the bond strength. The C—H bond strength was analyzed by the integral of crystal orbital Hamilton populations (ICOHP). The C—H bond in carbides is an essential factor in determining whether the trapped hydrogen atom is stable [76,77]. A lower value of ICOHP means a stronger bond [78–80]. The ICOHP results are shown in Fig. 9(c). After structural optimization, the *n*th unstable hydrogen atom would shift a short distance from trigonal interstitial to tetrahedral interstitial, making the C—H bond length longer and causing a lower C—H bond strength for the *n*th

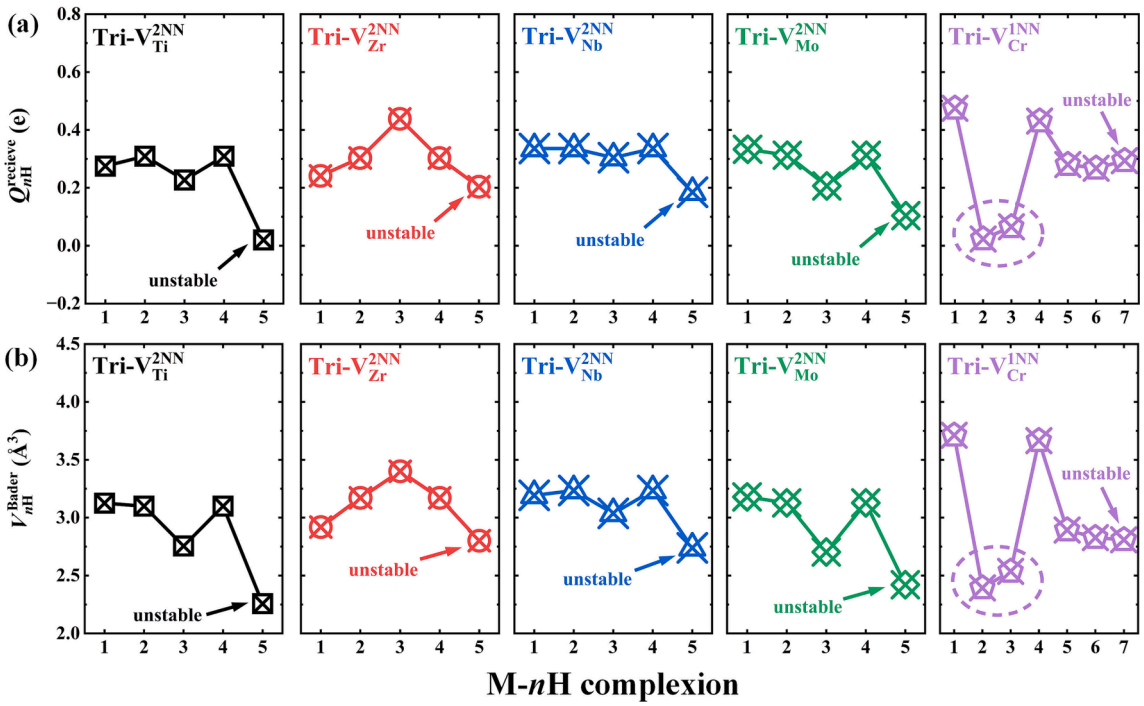


**Fig. 7.** Charge transfer and Bader volume of the stable and unstable hydrogen in M−*n*H complexion. (a) Charge transfer of hydrogen atom ($Q^{receive}_{nH}$), (b) Bader volume of hydrogen ($V^{Bader}_{nH}$).

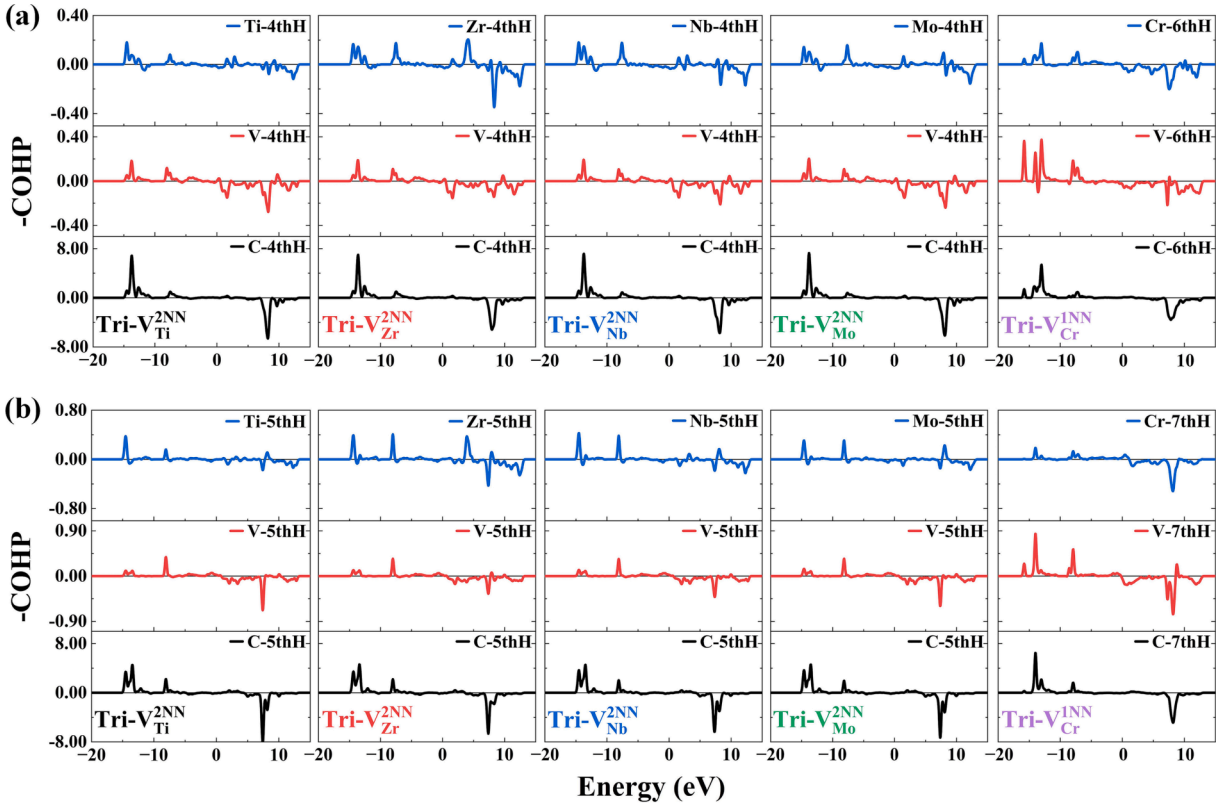


**Fig. 8.** Crystal orbital Hamiltonian population of stable and unstable hydrogen atoms in M−*n*H complexion. (a) Stable hydrogen atom, (b) unstable hydrogen atom.

unstable hydrogen atom than that for the stable hydrogen atom. This can explain the abrupt change in the mechanical and chemical effects of the solute atom and the *n*th unstable hydrogen atom.

The displacement of hydrogen atom from the trigonal interstitial to the tetrahedral interstitial results in a larger interstitial radius at the site occupied by the hydrogen atom. This leads to smaller lattice distortions, which weaken the adverse effects of the corresponding mechanical effects. While the displacement of hydrogen atom also leads to a reduction

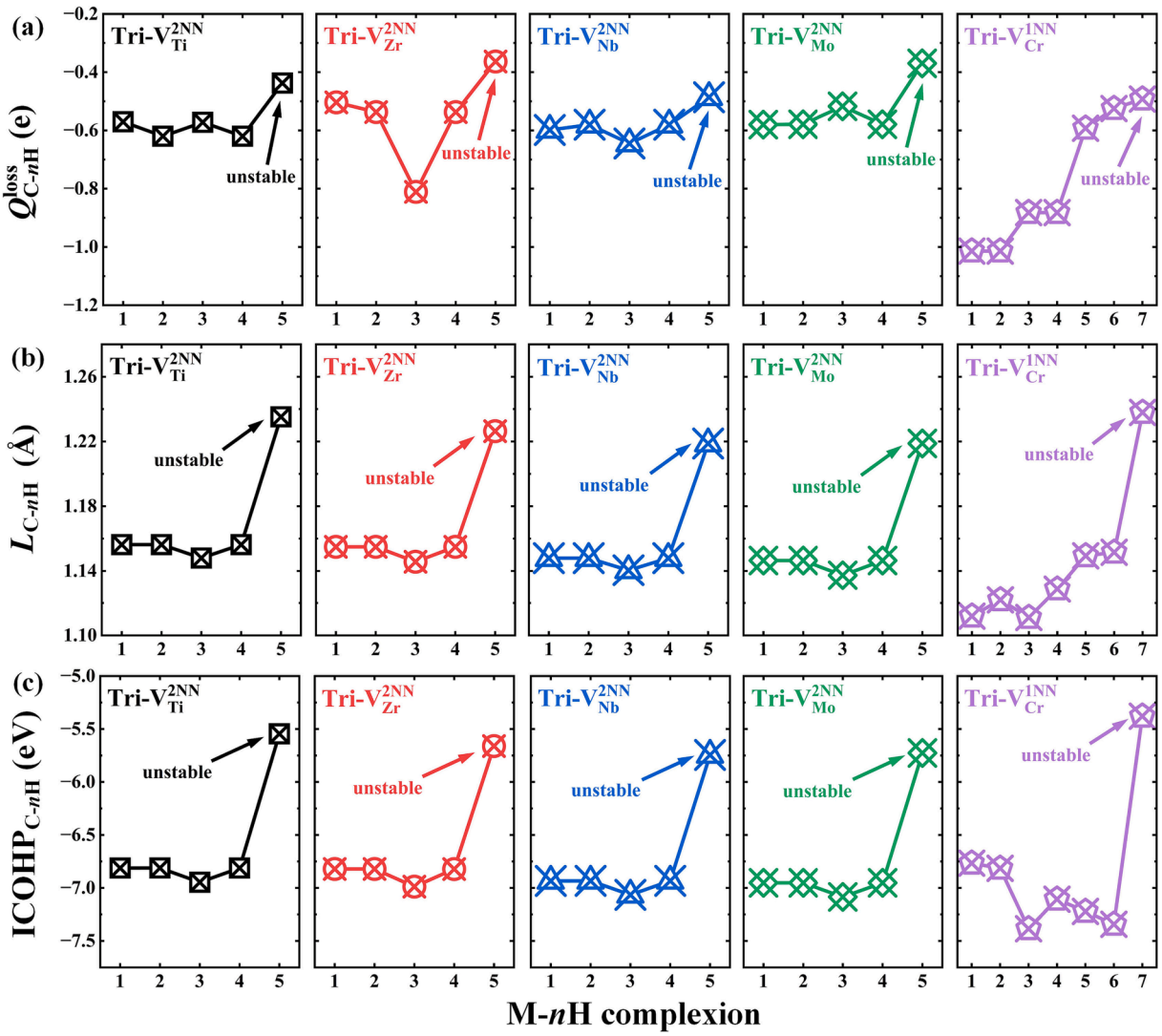


**Fig. 9.** Charge transfer of 1NN carbon atom, length and the integral of crystal orbital Hamilton populations value of the C—H bond in M−*n*H complexion. (a) Charge transfer of the 1NN carbon atom of hydrogen atom ($Q^{loss}_{C-nH}$). (b) C—H bond length ($L_{C-nH}$). (c) ICOHP value of C—H bond (ICOHP$_{C-nH}$). The numbers indicate the *n*th hydrogen atom added.

in the favorable effects of chemical effect. It can be understood as the hydrogen atom moving away from the most stable site. The chemical effect dominates the binding energy. As a result, the chemical effect of the *n*th unstable hydrogen atom is numerically greater relative to the most stable site. It can be concluded that the reason for the unstable hydrogen atom in doped VC is that the chemical environment substantially weakens the charge provided by the 1NN carbon atom to the unstable hydrogen atom and the strength of the C—H bond.

## Conclusions

The performance of the five transition-metal alloying atoms (Ti, Cr, Zr, Nb, and Mo) on the behavior of hydrogen trapping in vanadium carbide have been examined by means of first-principles calculations. The interaction between the H-H pairs in the VC has been scrutinized. The electronic structure analysis is used to rationalize the differences in the stable trapping sites for different solutes and the maximum trapping number. The hydrogen atom tends to occupy the second-nearest-neighbor (2NN) trigonal interstitial site in VC after doping the solute atoms (Ti, Zr, Nb, and Mo), while it changes to the first-nearest-neighbor one by the Cr doping.

Four hydrogen atoms can be stably trapped in the VC after doping the solute atoms (Ti, Zr, Nb, and Mo), while it becomes six hydrogen atoms after doping the Cr. The effects of the different doped atoms on the hydrogen trapping ability in VC are ordered by Cr > Zr > Nb > Ti > Mo. The doping of alloying elements can reduce the hydrogen permeability of the VC matrix by increasing the number of hydrogen trapped in the lattice, of which Cr is a good alloying element. The Cr has a distinct effect on the hydrogen trapping in the VC due to the less lattice contraction distortion from the smaller atomic radius of Cr and the lower loss of charge.

Charge transfer and the integral of crystal orbital Hamilton populations analyses indicate that the charge transfer from the carbon atom to the hydrogen atom affected by solute doping and the C—H bond strength is the main reason that the solute atoms cannot stably trap the *n*th hydrogen atom. Our results show that multi-component carbons can enhance the hydrogen trapping capacity of hydrogen barrier coatings. Our first-principles insights into the mechanism of multiple hydrogen trapping might benefit the material design of hydrogen barrier coatings for hydrogen energy and fusion energy.

## CRediT authorship contribution statement

**Shuai Tang:** Conceptualization, Formal analysis, Visualization,

Writing – original draft, Writing – review & editing. **Linxian Li:** Methodology, Investigation, Data curation, Visualization, Writing – original draft, Writing – review & editing. **Haile Yan:** Methodology, Investigation, Writing – review & editing. **Jianfeng Jin:** Methodology, Investigation. **Qing Peng:** Visualization, Formal analysis, Writing – review & editing. **Minghui Cai:** Investigation, Writing – review & editing. **Jianping Li:** Conceptualization, Supervision. **Zhenyu Liu:** Conceptualization, Supervision. **Guodong Wang:** Supervision.

## Declaration of Competing Interest

The authors declare that they have no known competing financial interests or personal relationships that could have appeared to influence the work reported in this paper.

## Data availability

Data will be made available on request.

## Acknowledgments

S. T. gratefully acknowledges the financial support of National Natural Science Foundation of China (Grant Nos. 52175293 and 51774083). Q. P. would like to acknowledge the support provided by National Natural Science Foundation of China (Grant No. 12272378), LiYing Program of the Institute of Mechanics, Chinese Academy of Sciences (Grant No. E1Z1011001) and Open Research Fund of State Key Laboratory of Rolling and Automation, Northeastern University (2022RALKFKT006). The authors acknowledge the 111 Project (Grant No. B20029).

## Appendix A. Supplementary material

Supplementary data to this article can be found online at https://doi.org/10.1016/j.nme.2023.101504.

## References

[1] K. Aoyagi, E.P. Torres, T. Suda, S. Ohnuki, Effect of hydrogen accumulation on mechanical property and microstructure of V-Cr–Ti alloys, J. Nucl. Mater. 283–287 (2000) 876–879, https://doi.org/10.1016/S0022-3115(00)00140-9.
[2] H.D.R. Hrig, J.R. Distefano, L.D. Chitwood, Effect of hydrogen and oxygen on the tensile properties of V–4Cr–4Ti, J. Nucl. Mater. 258–263 (1998) 1356–1360, https://doi.org/10.1016/S0022-3115(98)00201-3.
[3] J. Chen, Z. Xu, L. Yang, The influence of hydrogen on tensile properties of V-base alloys developed in China, J. Nucl. Mater. 307–311 (2002) 566–570, https://doi.org/10.1016/S0022-3115(02)01214-X.
[4] J.R. Distefano, J. Van, D.H. Röhrig, L.D. Chitwood, Reactions of hydrogen with V-Cr-Ti alloys, J. Nucl. Mater. 273 (1999) 102–110, https://doi.org/10.1016/S0022-3115(99)00014-8.
[5] Y. Asari, Y. Nakamura, Y. Tateyama, T. Ohno, H. Momida, Hydrogen-enhanced vacancy embrittlement of grain boundaries in iron, Phys. Rev. B 88 (14) (2013), 144107, https://doi.org/10.1103/PhysRevB.88.144107.
[6] P. Zhang, R. Li, J. Zhao, B. Wen, Synergetic effect of H and He with vacancy in vanadium solid from first-principles simulations, Nucl. Instrum. Methods Phys. Res. B 303 (2013) 75–80, https://doi.org/10.1016/j.nimb.2012.10.043.
[7] H. Matsui, K. Fukumoto, D.L. Smith, H.M. Chung, W. van Witzenburg, S. N. Votinov, Status of vanadium alloys for fusion reactors, J. Nucl. Mater. 233–237 (1996) 92–99, https://doi.org/10.1016/S0022-3115(96)00331-5.
[8] Y. Wu, S. Zhu, Y. Zhang, The adhesion strength and deuterium permeation property of SiC films synthesized by magnetron sputtering, Int. J. Hydrogen Energ. 41 (25) (2016) 10827–10832, https://doi.org/10.1016/j.ijhydene.2016.04.233.
[9] Y. Wu, L. Jiang, D. He, S. Li, Effect of Cr2O3 layer on the deuterium permeation properties of Y2O3/Cr2O3 composite coating prepared by MOCVD, Int. J. Hydrogen Energ. 41 (36) (2016) 16101–16107, https://doi.org/10.1016/j.ijhydene.2016.04.226.
[10] Y. Liu, S. Huang, J. Ding, Y. Yang, J. Zhao, Vanadium carbide coating as hydrogen permeation barrier: A DFT study, Int. J. Hydrogen Energ. 44 (12) (2019) 6093–6102, https://doi.org/10.1016/j.ijhydene.2019.01.049.
[11] S. Huang, W. Lo, Y. Yang, Vanadium carbide by MOCVD for mitigating the fuel cladding chemical interaction, Fusion Eng. Des. 125 (2017) 556–561, https://doi.org/10.1016/j.fusengdes.2017.04.118.
[12] Y. Ren, L. Li, Y. Zhou, S. Wang, In situ synthesized VC reinforced Fe-based coating by using extreme high-speed laser cladding, Mater. Lett. 315 (2022), 131962, https://doi.org/10.1016/j.matlet.2022.131962.
[13] X. Jiang, D. Zhao, Y. Wang, W. Duan, Toward hard yet tough VC coating via modulating compressive stress and nanostructure to enhance its protective performance in seawater, Ceram. Int. 45 (1) (2019) 1049–1057, https://doi.org/10.1016/j.ceramint.2018.09.284.
[14] Q. Wu, W. Li, N. Zhong, W. Gang, W. Haishan, Microstructure and wear behavior of laser cladding VC–Cr7C3 ceramic coating on steel substrate, Mater. Design 49 (2013) 10–18, https://doi.org/10.1016/j.matdes.2013.01.067.
[15] S. Huang, J. Tian, Y. Liu, Atomic study of hydrogen behavior in different vanadium carbides, J. Nucl. Mater. 554 (2021), 153096, https://doi.org/10.1016/j.jnucmat.2021.153096.
[16] L. Zhu, J. Luo, S. Zheng, S. Yang, J. Hu, Z. Chen, Understanding hydrogen diffusion mechanisms in doped α-Fe through DFT calculations, Int. J. Hydrogen Energ. 48 (46) (2023) 17703–17710, https://doi.org/10.1016/j.ijhydene.2023.01.150.
[17] H. Zhao, P. Chakraborty, D. Ponge, T. Hickel, B. Sun, C. Wu, B. Gault, D. Raabe, Hydrogen trapping and embrittlement in high-strength Al alloys, Nature 602 (7897) (2022) 437–441, https://doi.org/10.1038/s41586-021-04343-z.
[18] T. Tsuru, K. Shimizu, M. Yamaguchi, M. Itakura, K. Ebihara, A. Bendo, K. Matsuda, H. Toda, Hydrogen-accelerated spontaneous microcracking in high-strength aluminium alloys, Sci. Rep. 10 (1) (2020) 1998, https://doi.org/10.1038/s41598-020-58834-6.
[19] D.F. Johnson, E.A. Carter, Hydrogen in tungsten: Absorption, diffusion, vacancy trapping, and decohesion, J. Mater. Res. 25 (2) (2010) 315–327, https://doi.org/10.1557/JMR.2010.0036.
[20] X. Xiang, L. Zhu, F. Yang, L. Hu, G. Zhang, Fe effect on hydrogen interactions with intrinsic point defects and hydrogen migration in α-Al2O3 based tritium permeation barriers, J. Nucl. Mater. 542 (2020), 152494, https://doi.org/10.1016/j.jnucmat.2020.152494.
[21] X. Li, L. Chen, H. Liu, Z. Mi, C. Shi, L. Qiao, Atom doping in α-Fe2O3 thin films to prevent hydrogen permeation, Int. J. Hydrogen Energ. 44 (5) (2019) 3221–3229, https://doi.org/10.1016/j.ijhydene.2018.11.181.
[22] T. Kim, J. Lee, S. Kim, E. Hong, H. Lee, Hydrogen permeation barrier of carbon-doped TiZrN coatings by laser carburization, Corros. Sci. 190 (2021), 109700, https://doi.org/10.1016/j.corsci.2021.109700.
[23] V. Somjit, B. Yildiz, Doping α-Al2O3 to reduce its hydrogen permeability: Thermodynamic assessment of hydrogen defects and solubility from first principles, Acta Mater. 169 (2019) 172–183, https://doi.org/10.1016/j.actamat.2019.02.031.
[24] Y. Ma, Y. Shi, H. Wang, A first-principles study on the hydrogen trap characteristics of coherent nano-precipitates in α-Fe, Int. J. Hydrogen Energ. 45 (51) (2020) 27941–27949, https://doi.org/10.1016/j.ijhydene.2020.07.123.
[25] Y. Li, X. Zhang, T. Wu, First-principles study on the dissolution and diffusion behavior of hydrogen in carbide precipitates, Int. J. Hydrogen Energ. 46 (42) (2021) 22030–22039, https://doi.org/10.1016/j.ijhydene.2021.04.056.
[26] A. Nagao, M.L. Martin, M. Dadfarnia, P. Sofronis, I.M. Robertson, The effect of nanosized (Ti, Mo)C precipitates on hydrogen embrittlement of tempered lath martensitic steel, Acta Mater. 74 (2014) 244–254, https://doi.org/10.1016/j.actamat.2014.04.051.
[27] P. Dey, T. Hickel, J. Neugebauer, L. Sreekala, Unveiling nonmonotonic chemical trends in the solubility of H in complex Fe-Cr-Mn carbides by means of ab initio based approaches, Phys. Rev. Mater. 6 (1) (2022) 14403, https://doi.org/10.1103/PhysRevMaterials.6.014403.
[28] X. Jin, L. Xu, W. Yu, K. Yao, J. Shi, M. Wang, The effect of undissolved and temper-induced (Ti, Mo)C precipitates on hydrogen embrittlement of quenched and tempered Cr-Mo steel, Corros. Sci. 166 (2020), 108421, https://doi.org/10.1016/j.corsci.2019.108421.
[29] W.A. Counts, C. Wolverton, R. Gibala, First-principles energetics of hydrogen traps in α-Fe: Point defects, Acta Mater. 58 (14) (2010) 4730–4741, https://doi.org/10.1016/j.actamat.2010.05.010.
[30] A. Günen, B. Kurt, P. Milner, M.S. Gök, Properties and tribological performance of ceramic-base chromium and vanadium carbide composite coatings, Int. J. Refract. Hard Met. 81 (2019) 333–344, https://doi.org/10.1016/j.ijrmhm.2019.03.019.
[31] H. Cao, X.P. Dong, S. Chen, M. Dutka, Y. Pei, Microstructure evolutions of graded high-vanadium tool steel composite coating in-situ fabricated via atmospheric plasma beam alloying, J. Alloy. Compd 720 (2017) 169–181, https://doi.org/10.1016/j.jallcom.2017.05.226.
[32] C. Zhao, Y. Zhou, X. Xing, S. Liu, X. Ren, Q. Yang, Precipitation stability and micro-property of (Nb, Ti)C carbides in MMC coating, J. Alloy. Compd 763 (2018) 670–678, https://doi.org/10.1016/j.jallcom.2018.05.318.
[33] H. Dong, H. Chen, A. Riyahi Khorasgani, B. Zhang, Y. Zhang, Z. Wang, X. Zhou, W. Wang, H. Wang, T. Li, Z. Yang, S. van der Zwaag, Revealing the influence of Mo addition on interphase precipitation in Ti-bearing low carbon steels, Acta Mater. 223 (2022) 117475. 10.1016/j.actamat.2021.117475.
[34] C. Sun, Y. Zheng, L. Chen, F. Fang, X. Zhou, J. Jiang, Thermodynamic stability and mechanical properties of (V, M)C (M = W, Mo and Cr) multicomponent carbides: A combined theoretical and experimental study, J. Alloy. Compd 895 (2022), 162649, https://doi.org/10.1016/j.jallcom.2021.162649.
[35] D.G. Sangiovanni, F. Tasnádi, T. Harrington, M. Odén, Temperature-dependent elastic properties of binary and multicomponent high-entropy refractory carbides, Mater. Design 204 (2021), 109634, https://doi.org/10.1016/j.matdes.2021.109634.
[36] Y.S. Chen, H. Lu, J. Liang, Observation of hydrogen trapping at dislocations, grain boundaries, and precipitates, Science 367 (6474) (2020) 171–175, https://doi.org/10.1126/science.aaz0122.

[37] M. Koyama, M. Rohwerder, C.C. Tasan, Recent progress in microstructural hydrogen mapping in steels: quantification, kinetic analysis, and multi-scale characterisation, Mater. Sci. Technol. 33 (13) (2017) 1481–1496, https://doi.org/10.1080/02670836.2017.1299276.
[38] Q. Peng, G. Lu, Y. Sun, Quantum mechanical modeling of hydrogen assisted cracking in aluminum, Phys. Rev. B 88 (10) (2013), 104109, https://doi.org/10.1103/PhysRevB.88.104109.
[39] W. Counts, C. Wolverton, R. Gibala, Binding of multiple H atoms to solute atoms in bcc Fe using first principles, Acta Mater. 59 (14) (2011) 5812–5820, https://doi.org/10.1016/j.actamat.2011.05.058.
[40] M. Wei, X. Wang, P. Zhang, J. Zhao, P. Zheng, J. Chen, First-principles calculations of transition elements interaction with hydrogen in vanadium, J. Nucl. Mater. 564 (2022), 153710, https://doi.org/10.1016/j.jnucmat.2022.153710.
[41] J. Qin, Z. Liu, W. Zhao, D. Wang, Y. Zhang, Y. Zhong, X. Zhang, Z. Wang, C. Hu, J. Liu, Hydrogen Transportation Behaviour of V-Ni Solid Solution: A First-Principles Investigation, Materials 14 (2021) 2603, https://doi.org/10.3390/ma14102603.
[42] D.Y. Jiang, C.Y. Ouyang, S.Q. Liu, The effect of titanium(Ti) doping on hydrogen incorporation in tungsten(W):First-principles calculations, Fusion Eng. Des. 121 (2017) 227–234, https://doi.org/10.1016/j.fusengdes.2017.07.019.
[43] Y. Tateyama, T. Ohno, Stability and clusterization of hydrogen-vacancy complexes in α-Fe: An ab initio study, Phys. Rev. B 67 (17) (2003), 174105, https://doi.org/10.1103/PhysRevB.67.174105.
[44] K. Eguchi, H. Watanabe, M. Yamaguchi, M. Yagi, K. Ohsawa, Configuration and binding energy of multiple hydrogen atoms trapped in monovacancy in bcc transition metals, Phys. Rev. B 85 (9) (2012) 94102, https://doi.org/10.1103/PhysRevB.85.094102.
[45] Y. Zhang, H. Zhou, G. Lu, F. Liu, G.N. Luo, Y. Liu, Vacancy trapping mechanism for hydrogen bubble formation in metal, Phys. Rev. B 79 (17) (2009), 172103, https://doi.org/10.1103/PhysRevB.79.172103.
[46] J. Goto, M. Yamakami, M. Yamaguchi, M. Yagi, K. Ohsawa, Trapping of multiple hydrogen atoms in a tungsten monovacancy from first principles, Phys. Rev. B 82 (18) (2010), 184117, https://doi.org/10.1103/PhysRevB.82.184117.
[47] W. Xing, X. Chen, Q. Xie, G. Lu, D. Li, Y. Li, Unified mechanism for hydrogen trapping at metal vacancies, Int. J. Hydrogen Energ. 39 (21) (2014) 11321–11327, https://doi.org/10.1016/j.ijhydene.2014.05.032.
[48] B. Zhang, J. Su, M. Wang, Atomistic insight into hydrogen trapping at MC/BCC-Fe phase boundaries: The role of local atomic environment, Acta Mater. 208 (2021), 116744, https://doi.org/10.1016/j.actamat.2021.116744.
[49] R.L. Liu, D.Y. Li, Electron work function as an indicator for tuning the bulk modulus of MC carbide by metal-substitution: A first-principles computational study, Scr. Mater. 204 (2021), 114148, https://doi.org/10.1016/j.scriptamat.2021.114148.
[50] G. K. A, J. F. B, Efficiency of ab-initio total energy calculations for metals and semiconductors using a plane-wave basis set, Comp. Mater. Sci. 6 (1) (1996) 15-50. 10.1016/0927-0256(96)00008-0.
[51] J. Enkovaara, C. Rostgaard, J.J. Mortensen, J. Chen, Electronic structure calculations with GPAW: a real-space implementation of the projector augmented-wave method, J. Phys. Condens. Matter 22 (25) (2010), 253202, https://doi.org/10.1088/0953-8984/22/25/253202.
[52] J.P. Perdew, K. Burke, M. Ernzerhof, Generalized Gradient Approximation Made Simple, Phys. Rev. Lett. 77 (18) (1996) 3865–3868, https://doi.org/10.1103/PhysRevLett.77.3865.
[53] J.P. Perdew, J.A. Chevary, S.H. Vosko, Erratum: Atoms, molecules, solids, and surfaces: Applications of the generalized gradient approximation for exchange and correlation, Phys. Rev. B 48 (7) (1993) 4978, https://doi.org/10.1103/PhysRevB.48.4978.2.
[54] D.J. Chadi, Special points for Brillouin-zone integrations, Phys. Rev. B 16 (4) (1977) 1746–1747, https://doi.org/10.1016/10.1103/PhysRevB.16.1746.
[55] K. Ohsawa, K. Eguchi, H. Watanabe, Configuration and binding energy of multiple hydrogen atoms trapped in monovacancy in bcc transition metals, Phys. Rev. B 85 (9) (2012) 94102, https://doi.org/10.1103/PhysRevB.85.094102.
[56] K. Momma, F. Izumi, VESTA 3 for three-dimensional visualization of crystal, volumetric and morphology data, J. Appl. Crystallogr. 44 (2011) 1272–1276, https://doi.org/10.1107/S0021889811038970.
[57] W. Tang, E. Sanville, G. Henkelman, A grid-based Bader analysis algorithm without lattice bias, J. Phys Condens. Matter 21 (8) (2009) 84204, https://doi.org/10.1088/0953-8984/21/8/084204.
[58] V.L. Deringer, A.L. Tchougréeff, R. Dronskowski, Crystal Orbital Hamilton Population (COHP) Analysis As Projected from Plane-Wave Basis Sets, J. Phys. Chem. A 115 (21) (2011) 5461–5466, https://doi.org/10.1021/jp202489s.
[59] S. Tang, L. Li, Q. Peng, H. Yan, First-principles insights into hydrogen trapping in interstitial-vacancy complexes in vanadium carbide, Phys. Chem. Chem. Phys. 24 (34) (2022) 20400–20408, https://doi.org/10.1039/D2CP02425J.
[60] P. Zhang, T. Zou, J. Zhao, P. Zheng, J. Chen, Diffusion and retention of hydrogen in vanadium in presence of Ti and Cr: First-principles investigations, J. Nucl. Mater. 484 (2017) 276–282, https://doi.org/10.1016/j.jnucmat.2016.12.013.
[61] P. Zhang, C. Zhang, R. Li, J. Zhao, He-induced vacancy formation in bcc Fe solid from first-principles simulation, J. Nucl. Mater. 444 (1) (2014) 147–152, https://doi.org/10.1016/j.jnucmat.2013.09.048.
[62] O.I. Gorbatov, A.H. Delandar, Y.N. Gornostyrev, First-principles study of interactions between substitutional solutes in bcc iron, J. Nucl. Mater. 475 (2016) 140–148, https://doi.org/10.1016/j.jnucmat.2016.04.013.
[63] B. He, W. Xiao, W. Hao, Z. Tian, First-principles investigation into the effect of Cr on the segregation of multi-H at the Fe Σ3 (111) grain boundary, J. Nucl. Mater. 441 (1–3) (2013) 301–305, https://doi.org/10.1016/j.jnucmat.2013.06.015.
[64] U. Aydin, L. Ismer, T. Hickel, J. Neugebauer, Solution enthalpy of hydrogen in fourth row elements: Systematic trends derived from first principles, Phys. Rev. B 85 (15) (2012), 155144, https://doi.org/10.1103/PhysRevB.85.155144.
[65] H. Sawada, T. Omura, Interaction between hydrogen and solute atoms in bcc iron, Comp. Mater. Sci. 198 (2011) (2021), 110652, https://doi.org/10.1016/j.commatsci.2021.110652.
[66] Y. He, Y. Su, H. Yu, C. Chen, First-principles study of hydrogen trapping and diffusion at grain boundaries in γ-Fe, Int. J. Hydrogen Energ. 46 (10) (2021) 7589–7600, https://doi.org/10.1016/j.ijhydene.2020.11.238.
[67] S. Tang, L. Li, Q. Peng, H. Yan, Correction: First-principles insights into hydrogen trapping in interstitial-vacancy complexes in vanadium carbide, Phys. Chem. Chem. Phys. 24 (36) (2022) 22332, https://doi.org/10.1039/d2cp90165j.
[68] J. Pflüger, J. Fink, W. Weber, K.P. Bohnen, G. Crecelius, Dielectric properties of TiCx, TiNx, VCx, and VNx from 1.5 to 40 eV determined by electron-energy-loss spectroscopy, Phys. Rev. B 30 (3) (1984) 1155–1163, https://doi.org/10.1103/PhysRevB.30.1155.
[69] L. Chen, Y. Li, J. Peng, L. Sun, B. Li, Z. Wang, S. Zhao, A comparable study of Fe// MCs (M = Ti, V) interfaces by first-principles method: The chemical bonding, work of adhesion and electronic structures, J. Phys. Chem. Solids 138 (2020), 109292, https://doi.org/10.1016/j.jpcs.2019.109292.
[70] L. Zhang, H. Chen, X. Tao, H. Cai, J. Liu, Y. Ouyang, Q. Peng, Y. Du, Machine learning reveals the importance of the formation enthalpy and atom-size difference in forming phases of high entropy alloys, Mater. Des. 193 (2020), 108835, https://doi.org/10.1016/j.matdes.2020.108835.
[71] X. Kong, X. Wu, C.S. Liu, Q.F. Fang, Q.M. Hu, J. Chen, G.N. Luo, First-principles calculations of transition metal solute interactions with hydrogen in tungsten, Nucl. Fusion 56 (2) (2015) 26004, https://doi.org/10.1088/0029-5515/56/2/026004.
[72] P. Zhang, J. Zhao, B. Wen, Trapping of multiple hydrogen atoms in a vanadium monovacancy: A first-principles study, J. Nucl. Mater. 429 (1) (2012) 216–220, https://doi.org/10.1016/j.jnucmat.2012.06.018.
[73] H.J. Seo, Y. Heo, J.N. Kim, J. Lee, S. Choi, C.S. Lee, Effect of V/Mo ratio on the evolution of carbide precipitates and hydrogen embrittlement of tempered martensitic steel, Corros. Sci. 176 (2020), 108929, https://doi.org/10.1016/j.corsci.2020.108929.
[74] M.Y. Panchenko, G.G. Maier, I.A. Tumbusova, The effect of age-hardening mechanism on hydrogen embrittlement in high-nitrogen steels, Int. J. Hydrogen Energ. 44 (36) (2019) 20529–20544, https://doi.org/10.1016/j.ijhydene.2019.05.240.
[75] L.B. Peral, A. Zafra, I. Fernández-Pariente, Effect of internal hydrogen on the tensile properties of different CrMo(V) steel grades: Influence of vanadium addition on hydrogen trapping and diffusion, Int. J. Hydrogen Energ. 45 (41) (2020) 22054–22079, https://doi.org/10.1016/j.ijhydene.2020.05.228.
[76] X. Wang, C. Xu, S. Hu, H. Zhang, X. Zhou, S. Peng, The structure stability, diffusion behavior and elastic properties of stoichiometric ZrC bulk with interstitial hydrogen defect: A first-principles study, J. Nucl. Mater. 521 (2019) 146–154, https://doi.org/10.1016/j.jnucmat.2019.04.041.
[77] X. Yang, Y. Lu, P. Zhang, First-principles study of the stability and diffusion properties of hydrogen in zirconium carbide, J. Nucl. Mater. 479 (2016) 130–136, https://doi.org/10.1016/j.jnucmat.2016.07.008.
[78] N. Harshit, A. Roy, P.P. Chakrabarty, Jana, Site preference, atomic ordering, electronic structure and chemical bonding of A3Pd5 (A= Mg, Al, Ga): First principles study, Solid State Sci. 113 (2021), 106544, https://doi.org/10.1016/j.solidstatesciences.2021.106544.
[79] M. Ren, X. Guo, S. Huang, Transition metal atoms (Fe Co, Ni, Cu, Zn) doped RuIr surface for the hydrogen evolution reaction: A first-principles study, Appl. Surf. Sci. 556 (2021), 149801, https://doi.org/10.1016/j.apsusc.2021.149801.
[80] J. Wang, M. Enomoto, C. Shang, First-principles study on the P-induced embrittlement and de-embrittling effect of B and C in ferritic steels, Acta Mater. 219 (2021), 117260, https://doi.org/10.1016/j.actamat.2021.117260.